Nanotoxicology, December 2013; 7(8):1338–1350

ISSN: 1743-5390 print / 1743-5404 online
DOI: 10.3109/17435390.2012.739665

informa
healthcare

An *in vivo* and *in vitro* toxicological characterisation of realistic nanoscale CeO_2 inhalation exposures

Philip Demokritou[1], Samuel Gass[1], Georgios Pyrgiotakis[1], Joel M. Cohen[1], William Goldsmith[2], Walt McKinney[2], David Frazer[2], Jane Ma[2], Diane Schwegler-Berry[2], Joseph Brain[1], & Vincent Castranova[2]

[1]*Department of Environmental Health, Center for Nanotechnology and Nanotoxicology, Harvard School of Public Health, Harvard University, 665 Huntington Avenue, 02115 Boston, MA, USA and* [2]*National Institute for Occupational Safety and Health, Health Effects Laboratory Division, Pathology and Physiology Research Branch, Morgantown, WV, USA*

Abstract

Nanoscale CeO_2 is increasingly used for industrial and commercial applications, including catalysis, UV-shielding and as an additive in various nanocomposites. Because of its increasing potential for consumer and occupational exposures, a comprehensive toxicological characterisation of this nanomaterial is needed. Preliminary results from intratracheal instillation studies in rats point to cytotoxicity and inflammation, though these studies may not accurately use realistic nanoscale exposure profiles. By contrast, published *in vitro* cellular studies have reported limited toxicological outcomes for the case of nano-ceria. Here, the authors present an integrative study evaluating the toxicity of nanoscale CeO_2 both *in vitro*, using the A549 lung epithelial cell line, and *in vivo* using an intact rat model. Realistic nano-ceria exposure atmospheres were generated using the Harvard Versatile Engineered Nanomaterial Generation System (VENGES), and rats were exposed via inhalation. Finally, the use of a nanothin amorphous SiO_2 encapsulation coating as a means of mitigating CeO_2 toxicity was assessed. Results from the inhalation experiments show lung injury and inflammation with increased PMN and LDH levels in the bronchoalveolar lavage fluid of the CeO_2-exposed rats. Moreover, exposure to SiO_2-coated CeO_2 did not induce any pulmonary toxicity to the animals, representing clear evidence for the safe by design SiO_2-encapsualtion concept.

Keywords: engineered nanomaterials, CeO_2, *in vivo* inhalation studies, *in vitro* toxicological studies, safe by design ENMs

Introduction

The availability of cerium oxide as one of the most abundant rare-earth oxides has prompted research on the synthesis and development of functional CeO_2 nanoparticles (Ahrens 1995). As a result, nano-ceria is increasingly used in a variety of industrial and commercial applications including catalysis (Lawrence et al. 2011; Powell et al. 1988), chemical mechanical polishing (Kosynkin et al. 2000), UV-shielding (Dao et al. 2011) and as an additive in various nanocomposites. The inevitable increase in consumer and occupational exposures raises the need for a comprehensive toxicological characterisation of CeO_2 (Zhang et al. 2011). Many companies and organisations have already identified nano-CeO_2 as a high priority material for toxicological evaluations (OECD 2010). Assessing and understanding the interactions of nano-CeO_2 with environment and biological systems, as well as identifying means to reduce any potential toxicological outcomes, are therefore pivotal to the sustainability of industries employing nano-CeO_2 in their products.

While most *in vitro* cellular assays show minimal toxicity for nano-ceria particles (Hirst et al. 2009; Gass et al. 2013), preliminary results of *in vivo* animal models point to cytotoxicity and inflammation, as well as potential fibrogenicity (Nalabotu et al. 2011; Ma et al. 2011). These data, however, are limited to intratracheal instillation studies. It is worth pointing out that intratracheal or intranasal instillation or oropharyngeal aspiration deliver the total particle burden within a fraction of a second rather than over many hours, days or even weeks, as with inhalation exposure. Such bolus delivery may overwhelm local defence mechanisms and induce significant inflammatory effects that may not be seen when the same dose is administered over time by inhalation (Ma et al. 2011; Zhang et al. 2011). Bolus type deliveries of engineered nanomaterials (ENMs) dispersed in liquid media also result in significant changes to their physico-chemical properties due to agglomeration or protein corona effects that can alter their biological activity (Morimoto et al. 2012; Mercer et al. 2008;

Correspondence: Philip Demokritou, Department of Environmental Health, Center for Nanotechnology and Nanotoxicology, Harvard School of Public Health, Harvard University, 665 Huntington Avenue, 02115 Boston, MA, USA. Tel: +1 617 432 3481. Fax: +1 617 432 4710.
E-mail: pdemokri@hsph.harvard.edu and Vincent Castranova, National Institute for Occupational Safety and Health, Health Effects Laboratory Division, Pathology and Physiology Research Branch, Morgantown, WV, USA. Tel: +1 304 285 6056. Fax: +1 304 285 5938. E-mail: vic1@cdc.gov

(Received 20 July 2012; accepted 2 October 2012)

Wang et al. 2010; Cohen et al. 2013; Deloid et al. 2012, unpublished observations). To date, a whole-body *in vivo* inhalation study with realistic nano-ceria exposure atmospheres has yet to be performed.

Herein, an integrative and multifaceted study which focuses on three major research gaps related to biological properties of CeO_2 is presented. First, the toxicological implications of inhaled nano-CeO_2 exposures using an intact rat model are assessed. A realistic industry relevant CeO_2 aerosol was generated using the Harvard Versatile Engineered Nanomaterial Generating System (VENGES) recently developed by the authors (Demokritou et al. 2010; Sotiriou et al. 2011). The VENGES platform enables the synthesis of industry relevant, property-controlled ENM exposure atmospheres. More importantly, unlike other common aerosol generators used to disperse nanopowders for inhalation studies (e.g., nebulisers, fluidised beds and other venturi aspirator-type systems that have difficulty producing realistic nanosized aerosol distributions (Fischer & Chan 2007; Schmoll 2009)), exposure atmospheres generated here represent realistic industrial inhalation exposures to freshly generated CeO_2 ENMs. Second, a direct comparison between *in vivo* animal and *in vitro* cellular data was performed, shedding light on the ability of *in vitro* cellular assays to assess the safety of ENMs, using equivalent, comparable dose metrics. Particle deposition in the animal lungs was modelled using the Multiple Path Particle Deposition model (MPPD2) (Anjilvel & Asgharian 1995). The resulting lung dose was then converted to an equivalent *in vitro* administered dose using the recently developed *in vitro* sedimentation and diffusion dosimetry (ISDD) model (Hinderliter et al. 2010). Last, this study explores a safer by design concept for inhibiting nanoparticle toxicity based on a recently developed method by the authors involving the encapsulation of nanoparticles with an amorphous nanothin SiO_2 layer (Gass et al. 2013).

Methods

Realistic CeO_2 generation and animal exposure system

Figure 1 illustrates the CeO_2 synthesis and exposure system used in the study. It consists of the VENGES platform and the NIOSH (National Institute for Occupational Safety and Health) whole-body animal inhalation exposure system (Goldsmith et al. 2011). VENGES was used to generate the industry relevant, nanoscale CeO_2 aerosol exposures. ENMs were synthesised in the gas phase using a flame spray pyrolysis (FSP) reactor (Kammler et al. 2001) and collected on a water-cooled glass fibre filter for *ex situ* characterisation and *in vitro* cellular studies, as well as directed to exposure chambers for inhalation characterisation studies. The ability of VENGES to generate stable, real world, property controlled aerosols with full control over ENM primary particle and aggregate size was demonstrated in previous studies (Demokritou et al. 2010; Sotiriou et al. 2011). The VENGES platform was recently modified by the authors to enable in-flight coating of generated ENMs with a nanothin amorphous SiO_2 layer (Gass et al. 2013).

CeO_2 and SiO_2-coated CeO_2 nanomaterial synthesis

Uncoated CeO_2 particles and SiO_2-coated CeO_2 particles were synthesised by FSP of cerium (III) ethylhexanoate (0.05 M) dissolved in xylene and cerium (III) ethylhexanoate (0.04 M) dissolved in xylene:EHA (3:1), respectively. The precursor solutions were fed through a stainless steel capillary at 5 ml/min, dispersed by 5 l/min O_2 (Air Gas, purity >99%, pressure drop at nozzle tip: p_{drop} = 2 bar) and combusted to form the desired nanomaterial. A premixed stoichiometric methane-oxygen (1.5, 3.2 l/min) supporting flame was used in conjunction with 40 l/min O_2 (Air Gas, purity >99%) sheath gas. In the case of the synthesis of coated CeO_2, 16 l/min of pure N_2 was injected into the reactor through a torus ring with 16 equispaced and equisized (dinner = 0.6 mm) jets at an injection height of 200 mm above the FSP burner. In the case of SiO_2-coated CeO_2, 16 l/min N_2 carrying hexamethyldisiloxane (HMDSO, Sigma–Aldrich, St. Louis, MO, USA) vapour were fed through the same torus ring, this time, however, at injection height of 300 mm. HMDSO vapour was obtained by bubbling 0.11 l/min gas through liquid HMDSO (300 ml), maintained at 11.3°C using a temperature-controlled water bath. At saturation conditions, this corresponds to an HMDSO injection mass of 0.85 g/h into the reactor. In both cases, the reactor was enclosed above and below the torus ring by two quartz tubes (d_{inner} = 45 mm). More details on the synthesis of SiO_2-coated ENMs are provided in a recently submitted manuscript by the authors (Gass et al. 2013). Uncoated and SiO_2-coated CeO_2 ENMs were collected on a water-cooled glass fibre filter (Whatman) located 800 mm above the reactor (Figure 1) and used for off-line physico-chemical, morphological and *in vitro* cellular characterisation (see below for details).

Inhalation exposure system

The continuously generated aerosol was sampled *in situ* (Qs) by means of a peristaltic pump (Sarns, 3500), diluted with dry and filtered air (Qd), and subsequently fed to the whole-body inhalation chamber (Qs + Qd). A 150-L (22 × 22 × 20 inches) stainless steel whole-body exposure chamber (Cube 150) was used for this study (Goldsmith et al. 2011). The particle concentration (mass and number concentrations) in the chamber was controlled by adjusting the sampling to dilution flow rate ratio (typical dilution ratio was 1:15). Typical flow through the chamber was 21.7 l/min (Qd + Qs) with a corresponding residence time of approximately 7 min. Three stainless-steel 3/8-inch tubes were used as animal cage support exhaust ventilators. A stainless-steel cage rack, consisting of 12 individual wire mesh cages (5 × 7 × 3 inches) was placed on the supports. Exhaust holes were drilled in the bottom of the support (exhaust tubes) to minimise concentration gradients within the large exposure chamber and guarantee close to identical exposures for all animals within the cages (Goldsmith et al. 2011). The pressure in the chamber was maintained around 1 atm, by controlling the amount of air extracted from the chamber. Figure 1 shows the components and associated flows of the animal exposure system.

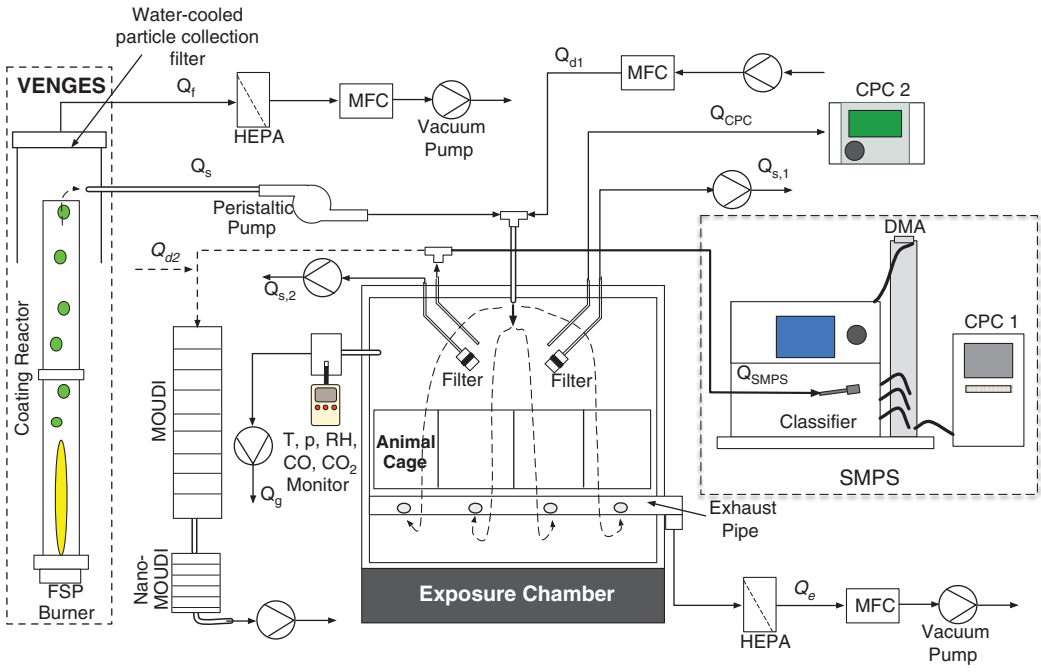

Legend

Symbol	*Definition*	*Specification**
VENGES	Versatile Engineered Nanomaterial Generation System	-
FSP	Flame Spray Pyrolysis	-
HEPA	High Efficiency Particulate Arresting	-
(Nano) MOUDI	Micro-Orifice Uniform Deposit Impactor	-
DMA	Differential Mobility Analyzer	-
CPC	Condensation Particle Counter	-
MFC	Mass Flow Controler	-
SMPS	Scanning Particle Mobility Sizer	-
Q_f	Main water-cooled Whatman filter flow	-
Q_s	In-situ sampling flow	15 l/.min
Q_{d1}	Particulate-free dilution flow	20.0 l/min
Q_g	Flow to gas, temperature and pressure monitor	3.0 l/min
Q_{CPC}	CPC sampling flow	1.0 l/min
$Q_{s,1(2)}$	In-situ filter measurement flow	3.0 l/min
Q_{SMPS}	Scanning mobility particle sizer flow	0.3 l/min
Q_{d2}	*Particulate-free dilution flow for MOUDI*	*15.0 l/min*
Q_m	*MOUDI flow*	*30.0 l/min*
Q_e	Chamber exhaust flow (to close mass balance)	-

Figure 1. ENM generation and inhalation exposure system. VENGES: Versatile Engineered Nanomaterial Generation System; FSP: flame spray pyrolysis; HEPA: High-Efficiency Particulate Air (Filter); MFC: mass flow controller; RH: relative humidity; p: pressure; T: temperature; SMPS: Scanning Mobility Particle Sizer; CPC: condensation particle counter; DMA: differential mobility analyser; MOUDI: Micro-Orifice Uniform Deposit Impactor.

Exposure monitoring and characterisation

Four sampling ports located directly over the animal breathing zone enabled real-time monitoring of exposure atmospheres. The real-time total number concentration in the chamber was monitored continuously by a condensation particle counter (CPC, Model #3775, TSI, Inc., Shoreview, MN, USA). Aerosol number concentration as a function of size was also monitored in real-time by a Scanning Mobility Particle Sizer (SMPS, Model 3080, TSI, Inc.). In addition, for the entire duration of the exposures, aerosol was sampled

from the exposure chamber for gravimetric analysis at a 3.5 l/min flow rate. ENMs were collected on a pre-weighed 37-mm Teflon filter (SKC, 0.45 μm pore size) housed in a closed-faced filter cassette. Filters were pre- and post-weighed (Mettler Toledo UMX2 Ultra Microbalance) in a relative humidity and temperature controlled environment (26–32% RH, 70–73 F). To verify no humidity effects, filters were also desiccated after post-weighing and then reweighed, showing negligible differences. Four filter measurements were taken each day of exposure.

In addition, separate experiments for both SiO_2-coated and uncoated CeO_2 exposure scenarios were performed in order to measure aerosol mass size distributions in the animal exposure chamber, using in series a Micro-Orifice Uniform Deposit Impactor (MOUDI, Model 110, MSP Corp., Minneapolis, MN, USA) (cut-point diameters: 0.056, 0.10, 0.18, 0.32, 0.56, 1.0, 1.8, 3.2, 5.6, 10, 18 μm) and a nano-MOUDI (MOUDI, Model 115, MSP Corp.) (cut-point diameters: 0.010, 0.018, 0.032 μm) (Figure 1). A set of 47-mm aluminium foil impaction substrates (MSP Corp.) were used for the gravimetric measurements. The 18 μm upper stage substrate was pre-coated with silicon oil to avoid particle bounce and contamination of size fractionated samples collected on lower stages.

The pressure inside the exposure chamber was also monitored continuously with a pressure transducer (Setra, Model 264). Exposure chamber temperature and relative humidity were also continuously monitored with a temperature/humidity sensor (Vaisala, Model 234). CO and CO_2 concentrations were monitored using a Q-Trak (TSI, Inc.).

ENM samples for field emission scanning and transmission electron microscopy (TEM/FESEM) were also collected *in situ* by sampling air from the exposure chamber (1.5 l/min) onto carbon grids (JOEL Model 1220 TEM, Hitachi Model S-4800 FESEM) with varying sampling time (120, 60, 30 and 10 s). ENMs were also deposited onto carbon grids, after sonication in ethanol, for higher resolution TEM imaging (TEM: Libra 120).

Ex situ characterisation of generated ENMs

ENMs collected on a water-cooled glass fibre filter (Figure 1) were extracted as nanopowders and used for both *ex situ* physico-chemical and morphological characterisation and *in vitro* cellular toxicological evaluation. X-ray diffraction (XRD) patterns were obtained using a Scintag XDS2000 powder diffractometer (Cu Kα (λ = 0.154 nm), -40 kV, 40 mA, step size = 0.02°). The crystal size was determined by applying the Scherrer Shape Equation to the Gaussian fit of the major diffraction peak. The Brunauer-Emmett-Teller (BET) powder-specific surface area (SSA) of all samples was measured by nitrogen adsorption at 77 K (Micromeritics TriStar), after sample degassing for 1 h at 150°C in nitrogen. BET equivalent primary particle size was calculated, under a spherical particle assumption, using $d_{BET} = 6000/(\rho \times SSA)$, where ρ is the material density. ENMs were also deposited onto carbon grids for TEM imaging (TEM: Libra 120) after 30 min sonication in ethanol. Highly surface sensitive X-ray photoelectron spectroscopy (XPS) (ESCA SSX-100, X-ray source: monochromatic Al Kα, 10 kV, 10 mA, detector: hemispherical electron energy spectrometer, spot size: 600 μm) was used to assess SiO_2 coating efficiency (Gass et al. 2013). Survey scans (binding energy range: 0–1100 eV, pass energy: 100 eV, step size: 0.65 eV), were used for surface elemental quantification. All XPS spectra were calibrated using the C1s hydrocarbon contamination peak (BE: 284.6 eV). Atomic concentrations were determined using CASA XPS software and respective sensitivity factors for relevant elements.

Toxicological characterisation of ENMs

Two different bio-assay systems were used to evaluate the toxicological profile of the generated ENMs: (1) *in vitro* cellular model, (2) *in vivo* animal model.

In vitro cellular assays

A number of standard viability/toxicity assays were employed to investigate ENM biointeractions *in vitro* across a range of physiologically relevant doses (0–100 μg/ml) on A549 lung epithelial cells. ENM preparation and characterisation in liquid suspension, cell culture methods and assay protocols are described in detail below.

ENM dispersal and characterisation in liquids

ENM dispersion was performed using a protocol previously developed by the authors and described elsewhere (Cohen et al. 2013), and included the calibration of sonication equipment and standardised reporting of sonication energy delivered by a Branson Sonifier S-450A (Branson Ultrasonics, Danbury, CT, USA) fitted with a 3 inch cup horn (maximum power output of 400 W at 60 Hz, continuous mode, output level 3). For each ENM the material-specific critical sonication energy required to achieve monodisperse solutions at the lowest agglomeration state as measured by dynamic light scattering (DLS) using a Zetasizer Nano-ZS (Malvern Instruments, Worcestershire, UK) was identified. Cup horn sonication was performed in deionised water (DI H_2O) to minimise reactive oxygen species generation via sonolysis, to minimise ionic strength and specific conductance, and hence particle interactions, during sonication, and to avoid denaturation of proteins in the final cell delivery media. Stock solutions in DI H_2O were then diluted to desired concentrations (0, 6.25, 12.5, 25, 50 or 100 μg/ml) in F-12K cell culture media supplemented with 3% heat-inactivated fetal bovine serum (FBS), 100 U/ml penicillin, 100 μg/ml streptomycin and 10 mM HEPES (F-12K/3%FBS) and vortexed for 30 s. ENM suspensions in F-12K/3%FBS were then characterised for hydrodynamic diameter (d_H), polydispersity index (PdI), zeta potential (ζ) and specific conductance (σ) by DLS, for pH using a VWR symphony pH meter (VWR International, Radnor, PA, USA), for effective density (ρ_E) by a recently developed volumetric centrifugation method (Deloid et al. 2012, unpublished observations), or applied to cells for toxicological evaluation.

Cell line

Human alveolar basal epithelial A549 cells were cultured in F-12K supplemented with 10% heat-inactivated FBS, 100 U/ml penicillin, 100 μg/ml streptomycin and 10 mM HEPES. All

incubations were performed at 37°C/5% CO_2 unless otherwise specified. Assays (see below) were repeated three times for each ENM. F-12K cell culture media, Penicillin/Streptomycin, HEPES and BSA were obtained from Sigma-Aldrich, and FBS and heat-inactivated FBS were obtained from Atlanta Biologicals (Atlanta, GA, USA).

Bio-assays

Cellular metabolic activity and cytotoxicity were measured via the 3-(4,5-dimethylthiazol-2-yl)-2,5-diphenyltetrazolium bromide (MTT) and lactate dehydrogenase (LDH) assay, respectively according to the standard protocols. In short, cells were seeded in 96-well microtiter plates (Corning Inc., New York, NY, USA) at a concentration of 1×10^5 cells per well. The next day, culture media was replaced with 100 µl of ENM dispersions in F-12K/3%FBS at various concentrations and incubated for 24 h. Following 24 h of exposure, 50 µl of supernatant was collected and transferred to fresh 96-well plates and 100 µl of LDH reagent was applied. These plates were then left for 30 min in the dark at room temperature. During this incubation period, the presence of LDH released by dead or dying cells into the supernatant due to plasma membrane damage was identified by the reduction of the reagent tetrazolium salt resulting in formazan, and measureable by absorbance. Plates were read immediately following incubation at 490 nm with a Synergy 2 Multi-Mode Microplate Reader (BioTek Instruments, Winooski, VT, USA).

Exposure media containing CeO_2 was removed from the plates still containing cells and replaced with fresh medium containing MTT reagent. These plates were then incubated for another 4 h. Vital cells integrated the dye and transformed the yellow tetrazolium salt (MTT) into purple formazan crystals, an indicator of active metabolism. Following the 4-h incubation period, 100 µl of MTT solubilisation solution (10% Triton X-100 with 0.1 N HCl in anhydrous isopropanol) were added to the wells to stop the reaction. Plates were placed on an orbital plate shaker for 30 min to dissolve the formazan crystals and then centrifuged at 250 rpm for 10 min to ensure that particles or dying cells were removed from the solution; 100 µl of the supernatant was then removed and placed in a fresh 96-well plate to be read at 570 nm with a Synergy 2 Multi-Mode Microplate Reader (BioTek Instruments). MTT Cell Proliferation kits and LDH Cytotoxicity Detection kits were obtained from Roche Applied Science (Indianapolis, IN, USA).

All experiments were conducted in triplicate for each ENM.

In vivo inhalation animal model

Male Sprague-Dawley rats (Hla: SD CVF, 8–10 weeks old) were obtained from Hilltop Labs (Scottdale, PA, USA). The animals were housed in the AAALAC-approved NIOSH Animal Facility (12 h light/dark cycle; 20–25°C), with food and water available *ad libitum*. Rats were acclimated to the facilities for 1 week prior to exposures. The NIOSH Animal Care and Use Committee approved all experimental procedures in this study. The animals ($n = 6$/group) were exposed to 2.7 mg/m^3 of either SiO_2-coated CeO_2, uncoated CeO_2 or particle-free environments (controls) (2 h/day, 4 days).

At 24 h post-exposure to ENMs, exposed animals, along with particle-free controls were anesthetised with sodium pentobarbital (0.2 g/kg, i.p.) and exsanguinated by cutting the renal artery. Alveolar macrophages (AM) were obtained by bronchoalveolar lavage (BAL) with a Ca^{2+}, Mg^{2+}-free phosphate buffered medium (145 mM NaCl, 5 mM KCl, 1.9 mM NaH_2PO_4, 9.35 mM Na_2HPO_4 and 5.5 mM glucose; pH 7.4) as described previously (Yang et al. 2001). Briefly, the lungs were lavaged with 6 ml Ca^{2+}, Mg^{2+}-free phosphate buffered medium for the first lavage, and subsequently lavaged with 8 ml of the same buffer for total 10 times or when total 80 ml BAL fluid were collected from each rat. The acellular supernate from the first lavage was saved separately from subsequent lavages for analysis of LDH activity and protein content. Cell pellets from each animal were centrifuged and combined, washed and resuspended in a HEPES buffered medium (145 mM NaCl, 5 mM KCl, 10 mM HEPES, 5.5 mM glucose and 1.0 mM $CaCl_2$; pH 7.4). Cell counts and purity were measured using an electronic cell counter equipped with a cell sizing attachment (Coulter model Multisizer II with a 256C channelizer; Beckman Coulter, Fullerton, CA, USA). Pathophysiological analysis was performed and inflammatory and cytotoxicity biomarkers including cell counts of polymorphonuclear neutrophils (PMNs) and AM, LDH activity and albumin content were measured in the first BAL fluid.

AM imaging: Rats were exposed to CeO_2, SiO_2-coated CeO_2 or vehicle by a single intratracheal instillation at a lung burden equivalent to that for the inhalation study (0.15 mg/kg). Rats were sacrificed at 1 day after exposure, BAL cells were isolated, fixed and particle uptakes were demonstrated by TEM (TEM: Libra 120).

Dosimetry considerations

Particle deposition in the animal lungs was modelled using the MPPD2 model (Anjilvel & Asgharian 1995). Table I summarises the parameters used in the simulations. An *in vivo* lung surface dose (µg/m^2) was estimated by integrating the highest model derived deposition flux (µg/(m^{2}min)) over the course of the exposure (min), which in this study was 480 min. The *in vitro* particle suspension volume to well surface ratio (ml/m^2) was then used to convert the *in vivo* lung surface dose (µg/m^2) to an *in vitro* equivalent volumetric dose (µg/ml). The underlying equation used was:

$$dose_{in-vitro,eq} = \dot{m}_{model} \times T_{\exp} \times \frac{A_{well}}{V_{ad\min}} \qquad (1)$$

where $dose_{in-vitro,eq}$ is the *in vitro* equivalent dose (µg/ml), $T_{\exp}$ is the total exposure time (min), $\dot{m}_{\mathrm{model}}$ is the highest model derived mass flux to the lungs (µg/(m^{2}min)), A_{well} is the surface area of the *in vitro* well (m^2) and V_{admin} is the volume of the media in one well (ml).

In order to convert the *in vitro* equivalent dose, which represents the delivered to cell dose to the equivalent administered dose, the *in vitro* sedimentation, diffusion and dosimetry (ISDD) model proposed by Hinderliter et al. (2010) was utilised in order to calculate numerically,

Table I. Summary of parameters used for *in vivo* lung deposition model (MPPD2).

Animal rat model	Breathing parameters	Particle properties
Functional residual capacity: 4.0 ml	Tidal volume: 2.1 ml	CMD: 90 nm (CeO_2), 100 nm (SiO_2-coated CeO_2)
Head volume: 0.42 ml	Breathing frequency: 102 l/min	Geometric standard deviation: 1.5
Breathing route: nasal	Inspiratory fraction: 0.5	Mass concentration: 2.7 mg/m^3
	Pause fraction: 0.0	

CMD, count mean diameter; MPPD2, Multiple Path Particle Deposition model.

for each ENM dispersion, the fraction of administered particles that would be deposited onto cells in a standard 96-well plate as a function of time $f_D(t)$. The particle hydrodynamic diameter (d_H, nm), as measured by DLS, and the measured effective density (ρ_E, g/cm^3) were used as inputs to the model (Deloid et al. 2012, unpublished observations). The effective density of ENMs in physiologic fluids was measured using the volumetric centrifugation method, which was recently developed by the authors (Deloid et al. 2012, unpublished observations). Additionally, the following parameters were used as input to the ISDD numerical model: media column height, 3.16 mm; temperature, 310K; media density, 1.00 g/ml; viscosity, 0.00074 Pa s (Hinderliter et al. 2010) and administered (initial suspension) particle concentration, 100 μg/ml.

Calculations and statistics

Absorbance values measured for LDH and MTT *in vitro* assays were normalised with negative control (particle-free media) and positive control (Triton X) absorbance values, to a metric of cell viability (%) using the following equation:

$$\text{Cell viability (\%)} = \frac{\text{Sample absorbance - negative control absorbance}}{\text{Positive control absorbance - negative control absorbance}}$$

Variance of toxicity results for each ENM was tested by *post hoc* one-way ANOVA with significance set at $p \leq 0.05$. One-tailed unpaired Student's *t*-test was used for significance testing, with significance set at $p \leq 0.05$.

Results

ENM characterisation

Figure 2 shows TEM and SEM images of CeO_2 and SiO_2-coated CeO_2 samples collected *in situ* (Figures 2C–F). The images illustrate the fractal structure of the agglomerates formed by the flame synthesis method. In the case of SiO_2-coated CeO_2, a smooth and relatively homogenous 2–4 nm SiO_2 coating layer is visible around the core CeO_2 particles at higher magnification (Figure 2G). The hermetic SiO_2 encapsulation of CeO_2 ENMs was also evaluated using XPS (Figure 2B). As shown in this figure, the Ce, 3d electron transition almost disappears entirely in the SiO_2-coated CeO_2 survey spectra. Small Ce 3d peaks that remain visible in the SiO_2-coated CeO_2 spectra can be attributed to a bulk Ce signal (Jung et al. 2003). This is in agreement with previous data that showed that coating thicknesses between 2 and 3 nm resulted in close to hermetic encapsulation of the core CeO_2 ENM (Gass et al. 2013). Figure 2A

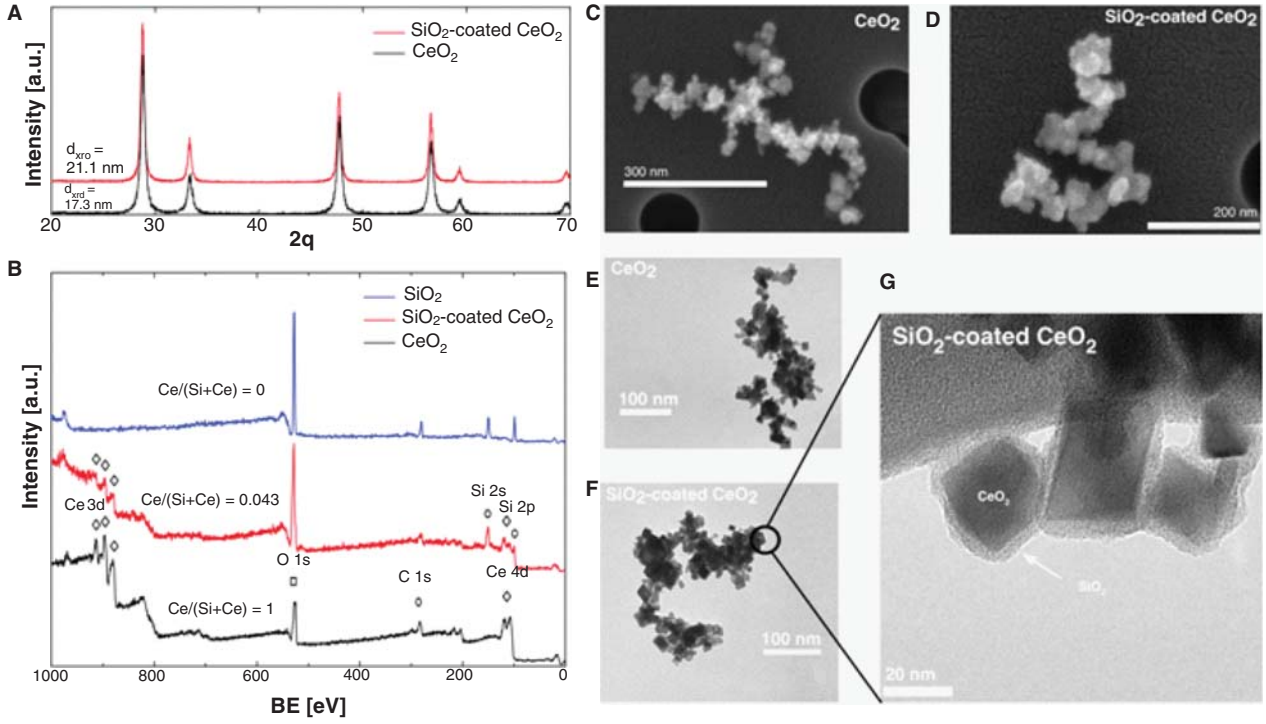

Figure 2. Physico-chemical ENM characterisation. XRD (A) and XPS (B) spectra of CeO_2 (black) and SiO_2-coated CeO_2 (red) (d_{XRD}: crystal size measured by X-ray diffraction). *In situ* SEM (C, D) and TEM (E, F) images of CeO_2 and SiO_2-coated CeO_2. Higher resolution TEM image of SiO_2-coated CeO_2 (*ex situ*); 2–4 nm SiO_2 coating appears as lighter contrast around darker contrast core CeO_2 particles (G).

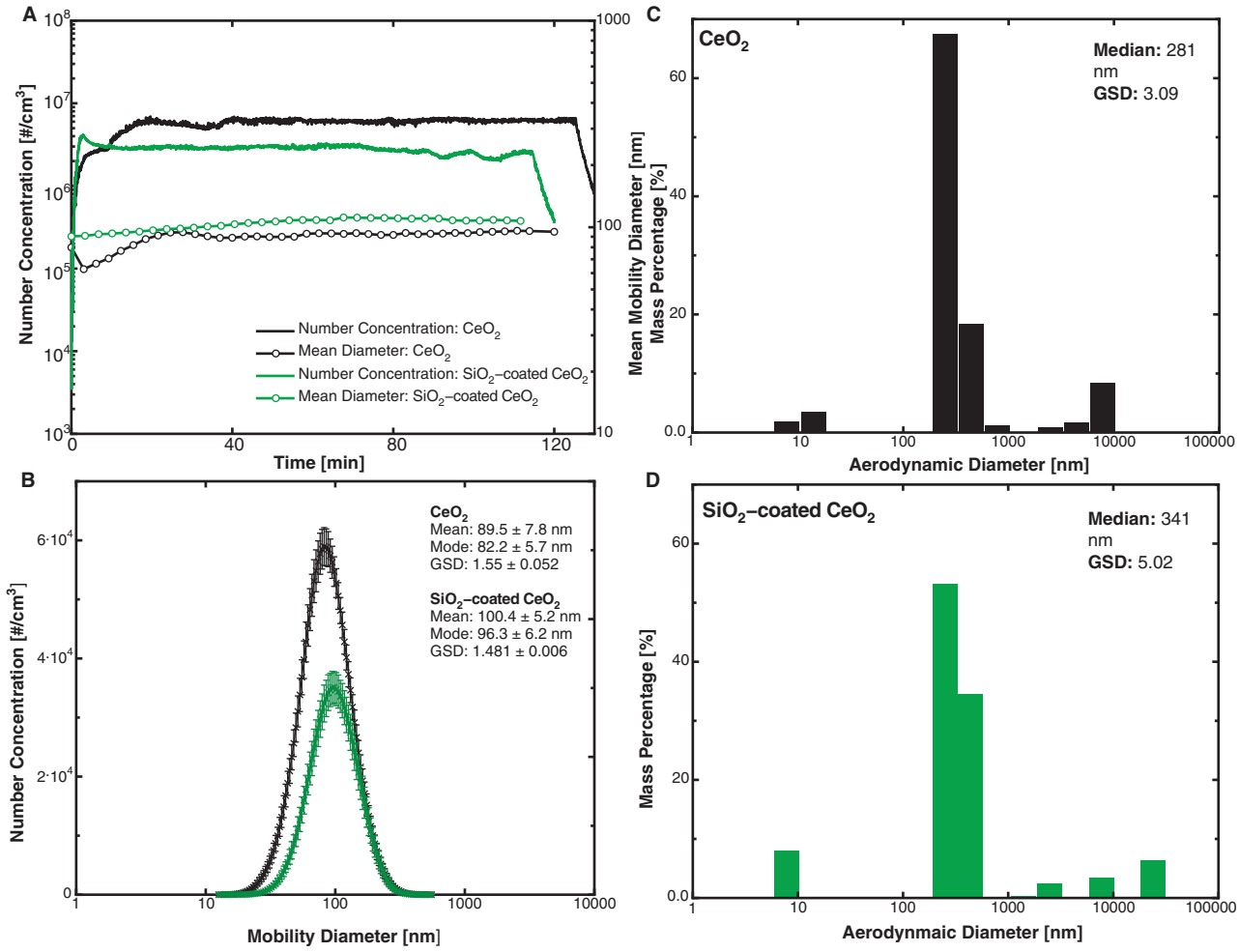

Figure 3. Inhalation exposure characterisation. (A) Total particle number concentration (solid line) and count mean diameter (CMD) (lines with circles) as a function of time for a representative 2 h exposure of CeO_2 (black) and SiO_2-coated CeO_2 (green). (B) Particle number concentration as a function of mobility diameter for CeO_2 (black) and SiO_2-coated CeO_2 (green) with corresponding distribution statistics. Error bars represent standard deviation over the entire course of the exposure (mean: count mean diameter; mode: count mode diameter; GSD: geometric standard deviation). MOUDI measured mass size distributions for uncoated CeO_2 (C) and SiO_2-coated CeO_2 (D) (median: mass median diameter; GSD: geometric standard deviation). The percentage of the total impacted mass is plotted for each aerodynamic diameter bin.

shows XRD patterns for CeO_2 and SiO_2-coated CeO_2. The location of the peaks is identical for both materials, indicating that the coating had minimal effect on core composition and crystal structure. XRD-determined crystal size of uncoated CeO_2 (17.3 nm) was slightly smaller than that of SiO_2-coated CeO_2 (21 nm). The SSA of uncoated CeO_2 was 61 m^2/g and the SSA of SiO_2-coated CeO_2 was 50 m^2/g, corresponding to an equivalent diameter of 12.8 and 19.2 nm, respectively. Differences between CeO_2 and SiO_2-coated BET equivalent diameter are more pronounced than crystal sizes due to SiO_2 encapsulation, which is not accounted for when measuring the crystal size.

In vivo animal inhalation experiments

Animal exposure characterisation

Figure 3A shows the total particle number concentration and mean aerosol mobility diameter as a function of time for a representative 2 h exposure experiment. Both number concentration and mean mobility diameter were remarkably constant over the 2 h exposure, highlighting the consistency and stability of the generation and exposure system. Figure 3B illustrates the aerosol number concentration in the animal exposure chamber as a function of mobility diameter for both the SiO_2-coated and uncoated CeO_2 exposure scenarios over the course of the exposure. It is worth pointing out that synthesis parameters were optimised in order to match aerosol size distributions for both SiO_2-coated and uncoated scenarios, since size distribution is an important determinant of lung deposition (Gangwal et al. 2011; Asgharian 2001). Statistics of the two aerosol distributions further prove this, as modal and geometric standard deviation diameters are almost identical for both SiO_2-coated and uncoated CeO_2. It should also be noted that the total number concentration was somewhat lower in the SiO_2-coated CeO_2 case, possibly due to slightly larger agglomerate sizes and denser agglomerates of higher effective densities.

Figures 3C and D illustrate the MOUDI measured mass size distributions for both SiO_2-coated and uncoated CeO_2 exposure scenarios. As with the particle number concentration distributions, the mass size distributions were also

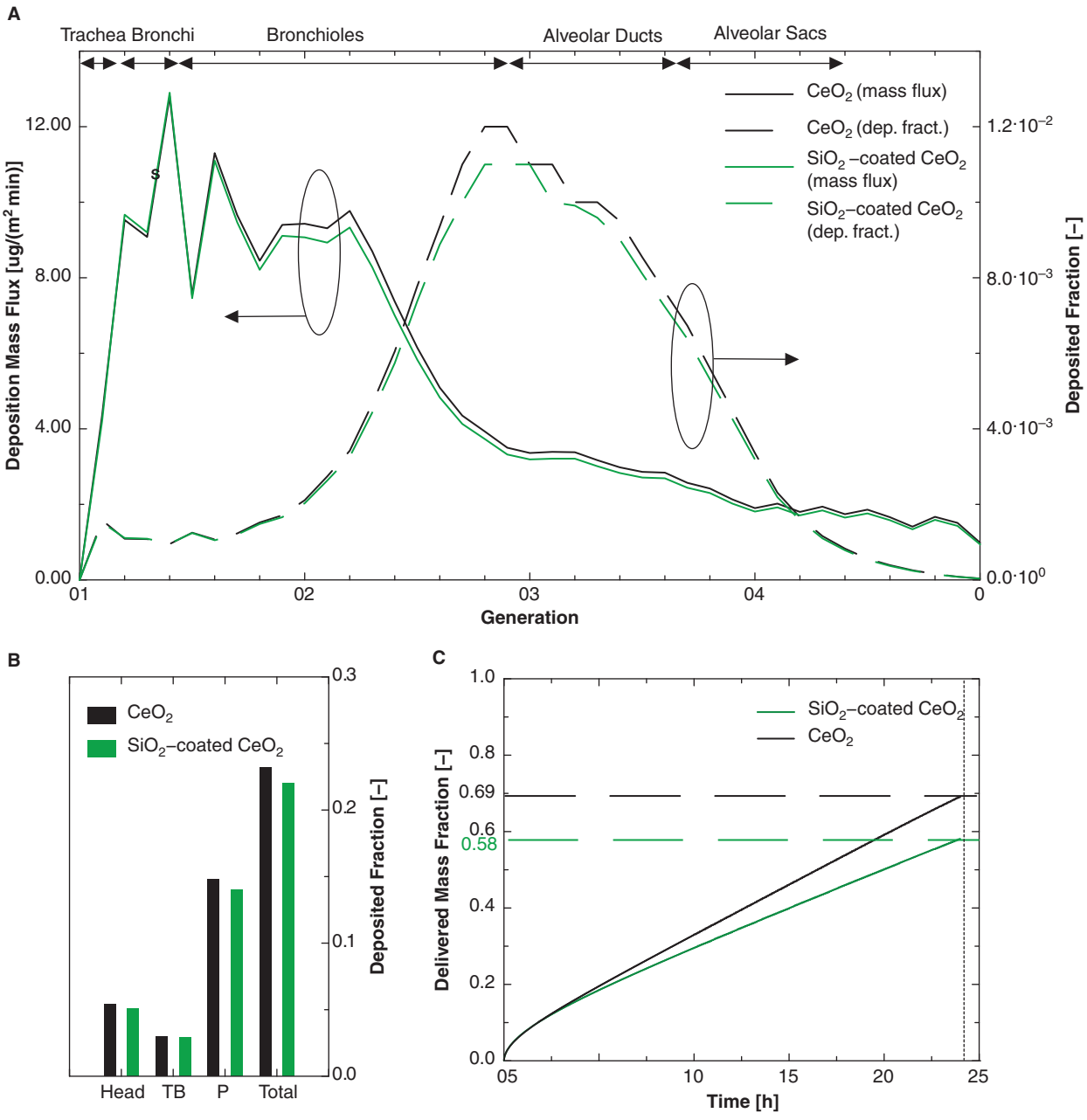

Figure 4. (A) Deposition mass flux (left axis) and deposition fraction (right axis) as a function of generation number. (B) Deposition fraction (dep. fract.) in total lung for head, tracheobronchial region (TB) and pulmonary region (P). (C) *In vitro* dosimetry: delivered mass fraction as a function of time for CeO_2 and SiO_2-coated CeO_2.

found to be similar, with most mass between 180 and 320 nm. Furthermore, gravimetric analysis of Teflon filters used throughout the duration of the exposures revealed an average mass concentration of 2.70 mg/m^3 for the CeO_2 scenario and 2.72 mg/m^3 for SiO_2-coated CeO_2 scenario in the animal exposure chamber. This is a clear indication that both number size distributions as well as mass concentration for both SiO_2-coated and uncoated exposure scenarios were well matched.

In addition, exposure chamber relative humidity and temperature were also similar and constant for both exposure scenarios, that is, 60% RH and 23.5°C. Similarly, the combustion off-gas concentrations (CO, CO_2) measured in the exposure chamber were very low and comparable with the concentrations in the particle-free control experiments.

Dosimetry considerations

Figure 4A shows the modelled deposited mass fraction in the animal lungs and the deposited mass flux for the different regions of the lung (shown as generation number) for both uncoated and SiO_2-coated CeO_2 ENMs. The model predicts deposition of most particle mass deeper in the animal lungs (higher generation numbers). This is somewhat expected given the small size of the CeO_2 exposures (Figure 3B). The deposition model also predicts almost identical deposition mass for both the CeO_2 and SiO_2-coated CeO_2 aerosol. Furthermore, based on a deposition mass flux of 12 μg/(m^{2}min) and an exposure time of 480 min, a lung surface dose of 5.76 × 10^3 μg/m^2 was estimated.

Equation 1 was used to calculate the equivalent *in vitro* dose delivered to cells, which was found to be 1.82 μg/ml

(well diameter = 6.35 mm, and media volume in a well = 0.1 ml). However, the *in vitro* dose delivered to cell is not the same as the administered dose (Cohen et al. 2013; Hinderliter et al. 2010) since only a fraction of the administered mass reaches the cells at the bottom of the well over time. The recently developed ISDD numerical model was used here to estimate the fraction of administered dose actually delivered to cells over time (Figure 4D) (Hinderliter et al. 2010; Deloid et al. 2012, unpublished observations). As shown in Figure 4C, only 69% of the CeO_2 particles, and 58% of the SiO_2-coated CeO_2 particles were delivered to cells over the course of the 24-h toxicity assay. Therefore, administered doses of 2.64 μg/ml for CeO_2 particles and 3.14 μg/ml for the SiO_2-coated CeO_2 are required to achieve the equivalent *in vitro* delivered to cell dose of 1.81 μg/ml which matches the *in vivo* equivalent dose of 5.76×10^3 μg/m^2.

Toxicological characterisation

In vivo animal inhalation experiments

Figure 5 summarises inflammatory and cytotoxicity biomarkers in the BAL fluid of the animals sacrificed one day post-exposure. While uncoated CeO_2 animal exposure induced considerable PMN infiltration compared with the control group, an indicator for inflammation, PMN levels for the SiO_2-coated scenario were similar to the particle-free control group levels (Figure 5B). Similarly, LDH release from the uncoated CeO_2-exposed group was significantly higher than the particle-free exposed control group, as shown in Figure 5D. It is known that LDH is a biomarker of cell damage and cytotoxicity. By contrast, LDH release in the SiO_2-coated CeO_2 exposed group was nearly identical to that of the particle-free exposed control group, clear evidence that the SiO_2 coating results in reduced toxicity (Figure 5D). Furthermore, both CeO_2 and SiO_2-coated exposures did not appear to cause air/capillary damage, as shown by similar albumin levels for SiO_2-coated, uncoated CeO_2 and the particle-free control animal group (Figure 5C). This is compelling evidence that the SiO_2 encapsulation significantly reduced particle toxicity.

In addition, as shown in the TEM micrographs presented in Figures 5E and F, CeO_2 and SiO_2-coated CeO_2 particles were present in both AM collected from CeO_2 and SiO_2-coated CeO_2 exposed animals, respectively. No particles were found in vehicle-exposed rats.

In vitro cellular characterisation

Comprehensive characterisation for each material dispersed in cell culture media is presented in Table II. As indicated in Table II, both the coated and uncoated CeO_2 particles exhibited narrow and monodisperse agglomerate size distributions, with mode around 200 nm in diameter, and effective densities close to 1.5 g/cm^3, when suspended in the biological media. Figure 6 reports the cell viability results from LDH and MTT assays for A549 cells for pure SiO_2, uncoated CeO_2 and SiO_2-coated CeO_2 particles for multiple administered dose levels (0–100 μg/ml, or 0–31.5 μg/cm^2 *in vivo* equivalent doses). As shown in Figures 6A and B, the viability of cells exposed to uncoated CeO_2, SiO_2-coated CeO_2 and pure SiO_2 particles was roughly equivalent to that observed for the negative control cells exposed only to particle-free cell-culture media. By contrast, the positive control cells exposed to Triton X exhibited minimal cell viability following 24 h of exposure (Figures 6A and B). It is worth mentioning here that results from the MTT assay presented in Figure 6 do exceed 100% for some doses, however, there is no statistical significance that might suggest that the values are truly different from the negative control or from each other (via ANOVA).

Discussion

This study showcases an integrative and multifaceted approach for evaluating the effect of realistic flame-generated nano-CeO_2 exposures on biological systems. Additionally, this study sheds light on major research gaps in the field of nanotoxicology. First, the authors assessed the toxicological implications of nano-CeO_2 exposure on an *in vivo* rat model using realistic freshly generated exposure atmospheres. Animal inhalation studies are considered the "gold standard" for pulmonary toxicology due to their physiologically relevant exposure mechanisms. According to the authors, this study represents the first whole-body *in vivo* animal inhalation study using realistic nano-scaled ceria exposure atmospheres.

Second, this study presents an interesting comparison between *in vivo* and *in vitro* cellular bioassays for the case of CeO_2. One major challenge of nanotoxicology is determining physiologically equivalent effective doses when comparing between *in vivo* and *in vitro* studies. To this end, the proposed approach can be used to match effective doses *in vitro* with their *in vivo* equivalents. However, even with perfectly matched *in vitro* and *in vivo* doses, results from this study suggest that widely used *in vitro* toxicity assays, such as LDH and MTT for A549 cells, may not be predictive of toxicological outcomes observed *in vivo* following inhalation exposure.

The CeO_2 inhalation toxicological results from this study indicated significant increase in LDH release compared with animals exposed to the particle-free control for the estimated effective dose of 5.76×10^3 μg/m^2 of lung surface area (Figure 5D). These results are in accordance with a recent intratracheal instillation study performed by the authors, which demonstrated that CeO_2 nanoparticles induced dose-dependent pulmonary inflammation and AM functional change in rats. In addition, further analysis revealed that CeO_2 particles activated the inflammatory macrophage (AM) phenotype, M1, as measured by increased IL-12 secretion and oxidant release (Ma et al. 2011).

By contrast, the anti-inflammatory nature of SiO_2 reported in a number of recently published *in vitro* studies (George 2011; Zhang et al. 2012) may explain the low lung injury and inflammation found in this study for the case of the SiO_2-coated CeO_2. In this study, when cells encountered amorphous SiO_2-coated CeO_2 they likely recognised the amorphous SiO_2 coating, not the CeO_2 core, thus resulting in much lower inflammation and cytotoxicity when compared with CeO_2. The biological inert nature of amorphous SiO_2 is documented in a number of *in vivo* studies. It was shown that

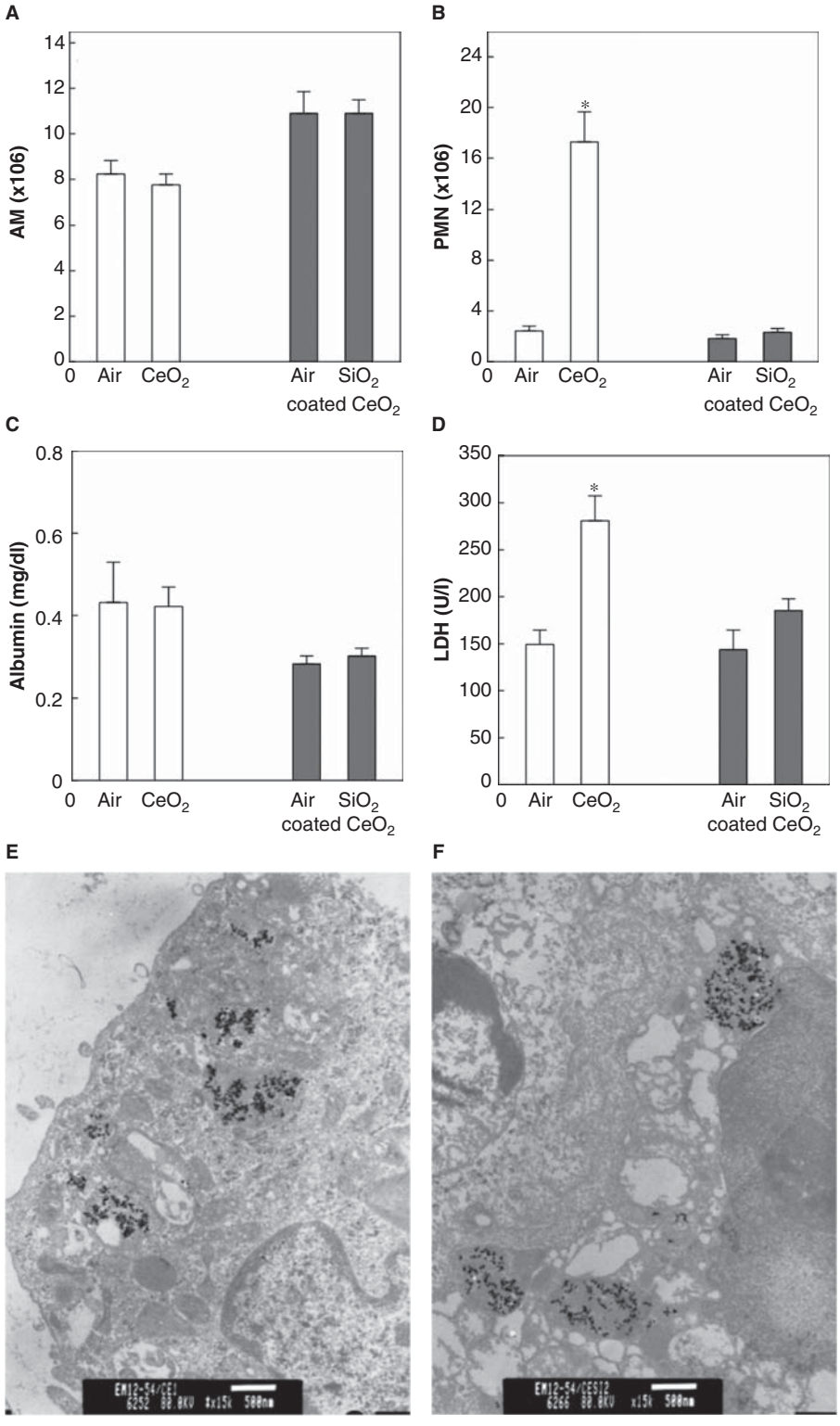

Figure 5. *In vivo* toxicity. Alveolar macrophages (AM) (A), polymorphonuclear neutrophils (PMNs) (B), albumin (C), lactate dehydrogenase (LDH) (D) levels in bronchoalveolar lavage (BAL) of rat sacrificed 1 day post-exposure. Error bars represent standard error, * represents p value < 0.05. Transmission electron microscopy (TEM) images of AM recovered from the BAL of rats instilled with CeO_2 (E) and SiO_2-coated CeO_2 particles (F).

amorphous SiO_2 induced a low and transient pulmonary inflammatory response in rats, whereas crystalline silica induced large and persistent pulmonary inflammatory responses (Warheit et al. 1995). It is also worth mentioning the differential pulmonary response associated with crystalline, colloidal or amorphous silica dusts (Warheit et al. 1995). Furthermore, recently published studies also suggest that amorphous SiO_2 is relatively insoluble in both water and in various cell culture media (Zhang et al. 2012).

It is also important to note that significant increases in PMN recruitment and LDH levels (a clear indication of lung injury and inflammation) without increased lung

Table II. Properties of ENM dispersions in F-12K/3%FBS.

Material	d_H (nm)	PdI	ζ (mV)	σ (mS/cm)	pH	ρ_E (g/cm^3)
CeO_2	241 ± 9.53	0.715 ± 0.055	-10.8 ± 1.57	14.1 ± 0.737	6.99 ± 0.074	1.54 ± 0
SiO_2-coated CeO_2	214 ± 6.16	0.246 ± 0.018	-10.8 ± 1.68	15.5 ± 1.70	6.89 ± 0.086	1.52 ± 0

d_H, hydrodynamic diameter; ENM, engineered nanomaterial; FBS, fetal bovine serum; PdI, polydispersity index; ζ, zeta potential; σ, specific conductance; ρ_E, effective density.

permeability, as measured by albumin levels (Figures 5B–D) may be associated with the low doses animals were exposed to in this study. Similar findings were reported in a previous study performed by the authors (Ma et al. 2011) for rats exposed to low doses of CeO_2 particles. On the contrary, at elevated exposure doses increased albumin levels in association with PMN recruitment and increased LDH were reported (Ma et al. 2011).

Interestingly, and in contrast to the *in vivo* inhalation data, no increase in LDH release was observed in A549 cells exposed to CeO_2 particles in liquid suspension, even at doses significantly higher than the estimated equivalent administered dose used *in vitro* of 2.64 μg/ml (equivalent to a delivered effective dose of 1.82 μg/ml, or 5.76 × 103 μg/m^2 *in vivo* dose) (Figure 6A). The authors do recognise that alternative *in vitro* assays, testing various end points across different cell lines, may improve sensitivity for detecting toxicity *in vitro* beyond the LDH and MTT assays reported here for A549 cells. However, several studies investigating the *in vitro* toxicity of CeO_2 across a broad range of cell lines from various tissues and examining a variety of biological end points have already been reported in the literature, and found CeO_2 to be relatively non-toxic across the board (Kroll et al. 2011a; Zhang et al. 2012; Xia et al. 2008).

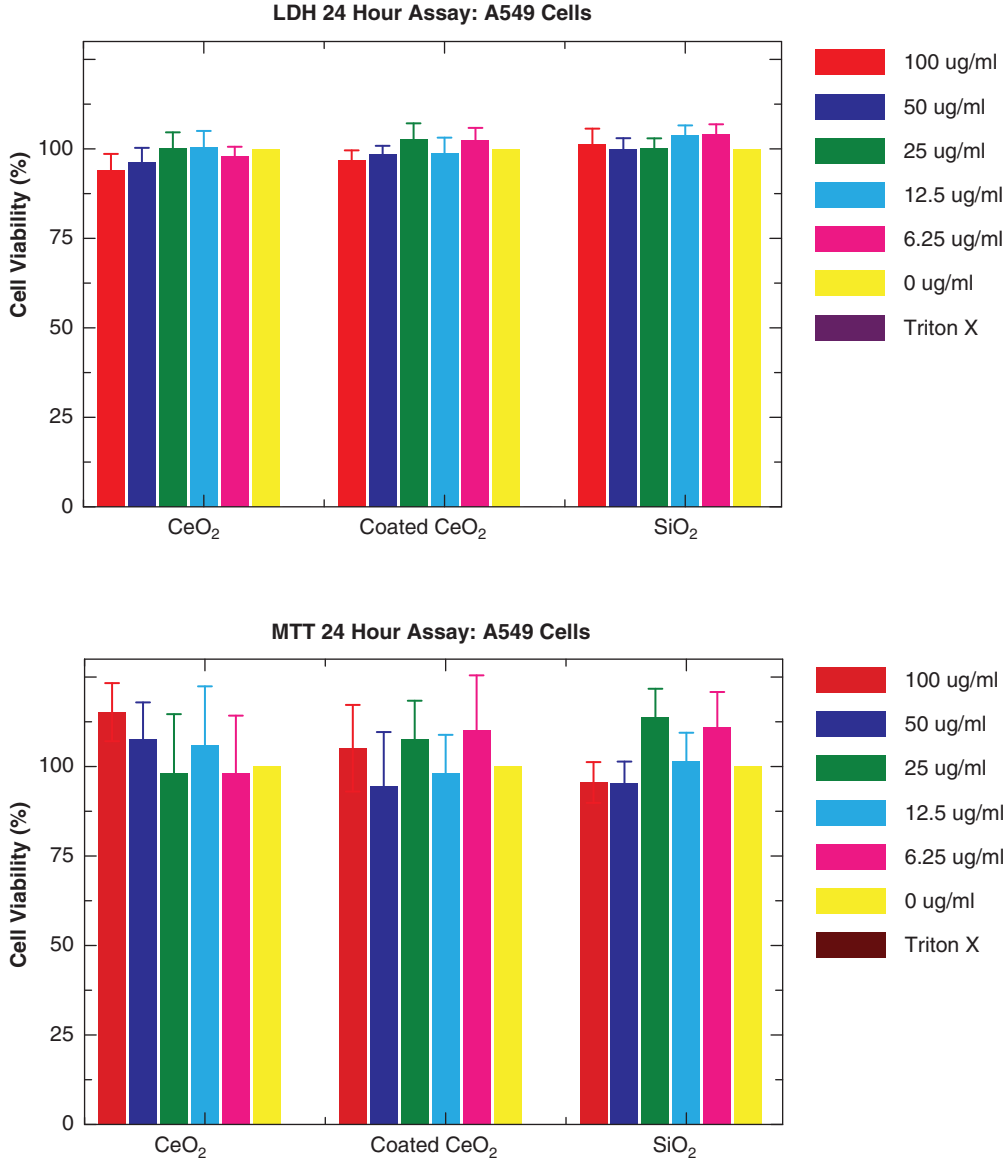

Figure 6. *In vitro* toxicity. Lactate dehydrogenase (LDH) and 3-(4,5-dimethylthiazol-2-yl)-2,5-diphenyltetrazolium bromide (MTT) absorbance after 24 h exposures to 0–100 μg/ml CeO_2 and SiO_2-coated CeO_2 in A549 cells. Error bars reflect standard deviation.

Specifically, Kroll et al. (2011a) reported that CeO_2 ENMs do not increase cell toxicity measured by LDH and MTT assays indicating membrane leakage and metabolic activity, and do not increase oxidative stress measured by reactive oxygen species generation by a DCF assay. Multiple cell lines were tested *in vitro* including A549 cells, heterogeneous human epithelial colorectal adenocarcinoma cells (Caco-2), adenocarcinoma-derived human lung epithelial cells (Calu-3), canine kidney epithelial cells (MDCK, MDCK II), mouse-derived fibroblast cells (NIH-3T3), rat kidney cells (NRK52E), rat AM (RAW 264.7) and rat lung epithelial-T-antigen negative cells (RLE-6TN). Similarly, Zhang et al. (2012) exposed multiple cell lines (human bronchial epithelial cells (BEAS-2B), and rat AM (RAW 264.7)) to CeO_2 particles and reported no increases in cell toxicity or oxidative stress. Inflammatory cytokine production may also be a more sensitive indicator of cellular responses to ENM exposure. However in the case of CeO_2, Xia et al. (2008) reported no increase in TNF-α production after the ENMs are internalised by rat AM (RAW 264.7), and no IL-8 production after they are internalised by non-cancerous human bronchial epithelial cells (BEAS-2B).

In conclusion, the *in vitro* results of this study are in accordance with the recent literature and a number of *in vitro* cellular studies, which suggest CeO_2 nanoparticles are relatively non-toxic (Xia et al. 2008; Kroll et al. 2011b; Raemy 2011). Some *in vitro* studies even suggest CeO_2 may reduce oxidative stress in cells, with potential therapeutic benefits for inflammation in humans (Hirst et al. 2009; Celardo et al. 2011). Discrepancies between *in vitro* and *in vivo* toxicity evaluations may be attributed to particle transformations in the micro-environments of cell culture media enriched with serum proteins versus the alveolar lining fluid of the animal lung. ENMs suspended in physiological media may experience agglomeration and the formation of a protein corona on the particle surface (Walkey & Chan 2012), and these transformations may mediate subsequent bio-nano interactions (Morimoto et al. 2012; Lundqvist et al. 2008; Syono et al. 1971). Future research will be necessary to determine just how much the protein corona and particle kinetics observed in an *in vitro* system can influence toxicity. One hypothesis to be investigated in future studies is whether distinct protein-particle interactions in cell culture media differ from those of alveolar lining fluid found in the animal lungs. Such a difference may explain some of the different biological responses between *in vitro* and *in vivo* reported in this study. Another possible explanation for the observed discrepancies between *in vitro* and *in vivo* results might be that single cell line *in vitro* assays lack interactions among the many cell types forming the lung epithelial barrier. Such interactions among different cell types may induce inflammation, and elicit further damage to the epithelial cells which cannot be captured by a single cell line assay (Kasper et al. 2011; Rothen-Rutishauser et al. 2005; Lehmann et al. 2011).

Finally, this study also explored a recently developed safety-by-design concept by the authors for inhibiting nanoparticle toxicity, based on the encapsulation of nanoparticles with an amorphous nanothin SiO_2 layer during their synthesis (Gass et al. 2013). It was clearly shown in this study that exposure to SiO_2-coated CeO_2 did not induce any pulmonary toxicity in a rat model. Thus, the results in this study provide valuable *in vivo* evidence for the safety of this SiO_2 encapsulation concept. Due to the scalability of this safer formulation concept, it bears great promise for large-scale industrial applications.

It is also worth pointing out that recent data from intratracheal instillation of CeO_2 nanoparticles in a rat model indicated that in addition to a rapid inflammatory/damage response, pulmonary fibrosis becomes evident at 3 months post-exposure (Ma et al. 2011). A number of exposed animals from this study were saved and will be sacrificed at 84 days post-exposure in order to further assess the fibrogenic behaviour of inhaled CeO_2. These fibrogenic responses along with extensive histopathology analysis of the lungs will be reported in a separate manuscript along with detailed biokinetic studies of CeO_2.

Acknowledgements

This study was supported by NIEHS (Grant # ES00000002) and NSF (ID# 1235806). The authors also gratefully acknowledge the generous financial support of BASF.

Declaration of interest

The findings and conclusions in this manuscript have not been formally disseminated by the NIOSH and should not be construed to represent any agency determination or policy.

References

Ahrens TJ. 1995. Global earth physics: a handbook of physical constants. American Geophysical Union: Washington DC.

Anjilvel S, Asgharian B. 1995. A multiple-path model of particle deposition in the rat lung. Toxicol Sci 28:41–50.

Asgharian B. 2001. Particle deposition in a multiple-path model of the human lung. Aerosol Sci Technol 34:8.

Celardo I, De Nicola M, Mandoli C, Pedersen JZ, Traversa E, Ghibelli L. 2011. Ce(3)+ ions determine redox-dependent anti-apoptotic effect of cerium oxide nanoparticles. ACS Nano 5:4537–4549.

Cohen J, Deloid G, Pyrgiotakis G, Demokritou P. 2013. Interactions of engineered nanomaterials in physiological media and implications for in vitro dosimetry. Nanotoxicology 7:417–431.

Dao NN, Luu MD, Nguyen QK, Kim BS. 2011. UV absorption by cerium oxide nanoparticles/epoxy composite thin films. Adv Nat Sci Nanosci Nanotechnol 2:045013.

Demokritou P, Buchel R, Molina RM, Deloid GM, Brain JD, Pratsinis SE. 2010. Development and characterization of a Versatile Engineered Nanomaterial Generation System (VENGES) suitable for toxicological studies. Inhal Toxicol 22(Suppl 2):107–116.

Fischer HC, Chan WC. 2007. Nanotoxicity: the growing need for in vivo study. Curr Opin Biotechnol 18:565–571.

Gangwal S, Brown JS, Wang A, Houck KA, Dix DJ, Kavlock RJ, et al. 2011. Informing selection of nanomaterial concentrations for ToxCast in vitro testing based on occupational exposure potential. Environ Health Perspect 119:1539–1546.

Gass S, Cohen JM, Pyrgiotakis G, Sotiriou GA, Buechel R, Pratsinis SE, et al. 2013. Safer formulation concept for flame-generated engineered nanomaterials. ACS Sustainable Chem Eng. DOI: 10.1021/sc300152f.

George S. 2011. Use of a high-throughput screening approach coupled with in vivo zebrafish embryo screening to develop hazard ranking for engineered nanomaterials. ACS Nano 5:13.

Goldsmith WT, Mckinney W, Jackson M, Law B, Bledsoe T, Siegel P, et al. 2011. A computer-controlled whole-body inhalation exposure system for the oil dispersant corexit Ec9500a. J Toxicol Environ Health A 74:1368–1380.

Hinderliter PM, Minard KR, Orr G, Chrisler WB, Thrall BD, Pounds JG, et al. 2010. ISDD: a computational model of particle sedimentation, diffusion and target cell dosimetry for in vitro toxicity studies. Part Fibre Toxicol 7:36.

Hirst SM, Karakoti AS, Tyler RD, Sriranganathan N, Seal S, Reilly CM. 2009. Anti-inflammatory properties of cerium oxide nanoparticles. Small 5:2848–2856.

Jung R, Lee JC, Orosz GT, Sulyok A, Zsolt G, Menyhard M. 2003. Determination of effective electron inelastic mean free paths in SiO2 and Si3N4 using a Si reference. Surf Sci 543:153–161.

Kammler HK, Madler L, Pratsinis SE. 2001. Flame synthesis of nanoparticles. Chem Eng Technol 24:14.

Kasper J, Hermanns MI, Bantz C, Maskos M, Stauber R, Pohl C, et al. 2011. Inflammatory and cytotoxic responses of an alveolar-capillary coculture model to silica nanoparticles: comparison with conventional monocultures. Part Fibre Toxicol 8:6.

Kosynkin VD, Arzgatkina AA, Ivanov EN, Chtoutsa MG, Grabko AI, Kardapolov AV, et al. 2000. The study of process production of polishing powder based on cerium dioxide. J Alloy Comp 303:421–425.

Kroll A, Dierker C, Rommel C, Hahn D, Wohlleben W, Schulze-Isfort C, et al. 2011a. Cytotoxicity screening of 23 engineered nanomaterials using a test matrix of ten cell lines and three different assays. Part Fibre Toxicol 8:9.

Kroll A, Dierker C, Rommel C, Hahn D, Wohlleben W, Schulze-Isfort C, et al. 2011b. Cytotoxicity screening of 23 engineered nanomaterials using a test matrix of ten cell lines and three different assays. Part Fibre Toxicol 8:9.

Lawrence NJ, Brewer JR, Wang L, Wu TS, Wells-Kingsbury J, Ihrig MM, et al. 2011. Defect engineering in cubic cerium oxide nanostructures for catalytic oxidation. Nano Letters. 11:2666–2671.

Lehmann AD, Daum N, Bur M, Lehr CM, Gehr P, Rothen-Rutishauser BM. 2011. An in vitro triple cell co-culture model with primary cells mimicking the human alveolar epithelial barrier. Eur J Pharm Biopharm 77:398–406.

Lundqvist M, Stigler J, Elia G, Lynch I, Cedervall T, Dawson KA. 2008. Nanoparticle size and surface properties determine the protein corona with possible implications for biological impacts. Proc Natl Acad Sci USA 105:14265–14270.

Ma JY, Zhao HW, Mercer RR, Barger M, Rao M, Meighan T, et al. 2011. Cerium oxide nanoparticle-induced pulmonary inflammation and alveolar macrophage functional change in rats. Nanotoxicology 5:312–325.

Mercer RR, Scabilloni J, Wang L, Kisin E, Murray AR, Schwegler-Berry D, et al. 2008. Alteration of deposition pattern and pulmonary response as a result of improved dispersion of aspirated single-walled carbon nanotubes in a mouse model. Am J Physiol Lung Cell Mol Physiol 294:L87–L97.

Morimoto Y, Horie M, Kobayashi N, Shinohara N, Shimada M. 2012. Inhalation Toxicity Assessment of Carbon-Based Nanoparticles. Acc Chem Res. doi: 10.1021/ar200311b.

Nalabotu SK, Kolli MB, Triest WE, Ma JY, Manne ND, Katta A, et al. 2011. Intratracheal instillation of cerium oxide nanoparticles induces hepatic toxicity in male Sprague-Dawley rats. Int J Nanomedicine 6:2327–2335.

OECD. 2010. List of manufactured nanomaterials and list of endpoints for phase one of the OECD testing programme. Series on the Safety of Manufactured Nanomaterials No. 6. Paris.Available at http://www.oecd.org/science/safetyofmanufacturednanomaterials/publicationsintheseriesonthesafetyofmanufacturednanomaterials.htm

Powell BR, Bloink RL, Eickel CC. 1988. Preparation of cerium dioxide powders for catalyst supports. J Am Ceramic Soc 71:C-104–C-106.

Raemy DEA. 2011. Cerium oxide nanoparticle uptake kinetics from the gas-phase into lung cells in vitro is transport limited. Eur J Pharm Biopharm 77:8.

Rothen-Rutishauser BM, Kiama SG, Gehr P. 2005. A three-dimensional cellular model of the human respiratory tract to study the interaction with particles. Am J Respir Cell Mol Biol 32:281–289.

Schmoll LH. 2009. Nanoparticle aerosol generation methods from bulk powders for inhalation exposure studies. Nanotoxicology 3:11.

Sotiriou GA, Diaz E, Long MS, Godleski J, Brain J, Pratsinis SE, et al. 2011. A novel platform for pulmonary and cardiovascular toxicological characterization of inhaled engineered nanomaterials. Nanotoxicology 6:680–90.

Syono Y, Akimoto SI, Matsui Y. 1971. High pressure transformations in zinc silicates. J Solid State Chem 3:369–380.

Walkey CD, Chan WC. 2012. Understanding and controlling the interaction of nanomaterials with proteins in a physiological environment. Chem Soc Rev 41:2780–2799.

Wang L, Castranova V, Mishra A, Chen B, Mercer RR, Schwegler-Berry D, et al. 2010. Dispersion of single-walled carbon nanotubes by a natural lung surfactant for pulmonary in vitro and in vivo toxicity studies. Part Fibre Toxicol 7:31.

Warheit DB, Mchugh TA, Hartsky MA. 1995. Differential pulmonary responses in rats inhaling crystalline, colloidal or amorphous silica dusts. Scand J Work Environ Health 21(Suppl 2):19–21.

Xia T, Kovochich M, Liong M, Madler L, Gilbert B, Shi H, et al. 2008. Comparison of the mechanism of toxicity of zinc oxide and cerium oxide nanoparticles based on dissolution and oxidative stress properties. ACS Nano 2:2121–2134.

Yang HM Antonini JM, Barger MW, Butterworth L, Roberts BR, MA JK, Castranova V, MA JY 2001. Diesel exhaust particles suppress macrophage function and slow the pulmonary clearance of Listeria monocytogenes in rats. Environ Health Perspect 109: 515–21.

Zhang H, He X, Zhang Z, Zhang P, Li Y, Ma Y, et al. 2011. Nano-CeO2 exhibits adverse effects at environmental relevant concentrations. Environ Sci Technol 45:3725–3730.

Zhang H, Ji Z, Xia T, Meng H, Low-Kam C, Liu R, et al. 2012. Use of metal oxide nanoparticle band gap to develop a predictive paradigm for oxidative stress and acute pulmonary inflammation. ACS Nano 6:4349–4368.

NOTICE OF CORRECTION

The iFirst version of this article published online ahead of print on 09 November 2012 contained an error in reference citations Gass et al. and Deloid et al. The citation "Gass et al." should be updated as "Gass et al. 2013" and "Deloid et al." should read "Deloid et al." unpublished observations. The corrected version is shown in this issue.